Biochimica et Biophysica Acta (BBA) - Biomembranes.
Volume 1862, Issue 5, 1 May 2020, 183188
https://doi.org/10.1016/j.bbamem.2020.183188

Sensing molecular organizational changes through the catalytic activity of acetylcholinesterase from erythrocyte membranes in Langmuir-Blodgett films.

Iván Felsztyna[1,2], Anahí V. Turina[1,2], María A. Perillo[1,2,*] and Eduardo M. Clop[1,2,*]

[1] Universidad Nacional de Córdoba, Facultad de Ciencias Exactas, Físicas y Naturales. Departamento de Química, Cátedra de Química Biológica. Córdoba, Argentina.

[2] CONICET, Instituto de Investigaciones Biológicas y Tecnológicas (IIByT). Córdoba, Argentina

∗ Co-corresponding authors:

e-mail: eduardo.clop@unc.edu.ar; mperillo@unc.edu.ar

Biochimica et Biophysica Acta (BBA) - Biomembranes.
Volume 1862, Issue 5, 1 May 2020, 183188
https://doi.org/10.1016/j.bbamem.2020.183188

Highlights

Bovine **E**rythrocyte **M**embrane (BEM) forms stable liquid-expanded Langmuir films (LF_{BEM})

Langmuir-Blodgett films (LB_{BEM}) are successfully built from LF_{BEM}.

LB_{BEM} retain the activity of **B**ovine **E**rythrocyte **A**cetylcholinesterase (BEA)

BEA catalytic activity serves to probe the molecular packing and dynamics in LB_{BEM}

LB_{BEM} may stand for a prototype of an optical biosensor for monoterpene pesticides.

Biochimica et Biophysica Acta (BBA) - Biomembranes.
Volume 1862, Issue 5, 1 May 2020, 183188
https://doi.org/10.1016/j.bbamem.2020.183188

Abstract

Langmuir films prepared from bovine erythrocyte membranes (LF_{BEM}) were studied and transferred to alkylated glasses (Langmuir-Blodgett films, LB_{BEM}) in order to assess the effects of membrane molecular packing on **B**ovine **E**rythrocyte **A**cetylcholinesterase (BEA) catalytic activity.

Surface pressure (π) vs Area isotherms showed three 2D-transitions at ~7, ~18 and ~44 mN/m and a collapse pressure at π_c=49 mN/m. The 0-12-0 mN/m compression-decompression cycles resulted reversible while those 0-40-0 mN/m exhibited a significant hysteresis. Taken together EFM, BAM and AFM images and the stability of the film after 3 C-D cycles, we can suggest that over the air-water interface as well as over the silanized glass substrate the surface is mostly covered by a monolayer with a few particles dispersed.

Acetylthiocholine hydrolysis was assayed with BEA in bovine erythrocyte membrane suspensions (S_{BEM}) and in LB_{BEM} packed at 10 ($LB_{BEM,10}$) and 35 mN/m ($LB_{BEM,35}$), which gave the following kinetic parameters: V_{max}= 3.41±0.15, 0.021±0.002 and 0.030±0.003 nmol.min^{-1}·µg prot^{-1} and K_M=0.11±0.02, 0.047±0.017 and 0.026±0.017 mM, respectively. Although from S_{BEM} to LB_{BEM} we lost active enzyme, the catalytic efficiency (V_{max}/K_M) increased ~750 times. Eugenol and 1,8-cineol inhibited BEA catalytic activity in $LB_{BEM,35}$.

Our results demonstrate the transmission of information between the membrane and the environment within the subphase immediately below the membrane, where anchored proteins are hosted. This was reflected by the membrane packing-induced modulation of BEA catalytic activity.

Furthermore, LB_{BEM} provides a proof of concept for the development of biosensors to screen new green pesticides acting through BEA interaction.

Keywords

Erythrocyte acetylcholinesterase; bovine erythrocyte membranes, Langmuir-Blodgett films; monoterpenes; biosensor proof of principle

Biochimica et Biophysica Acta (BBA) - Biomembranes.
Volume 1862, Issue 5, 1 May 2020, 183188
https://doi.org/10.1016/j.bbamem.2020.183188

Graphical Abstract

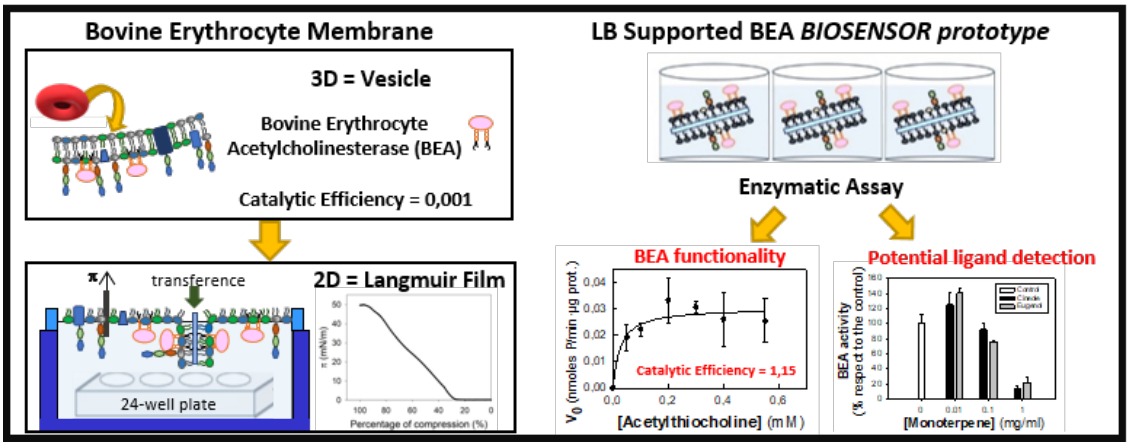

Bovine erythrocyte acetylcholinesterase (BEA) in Langmuir Blodgett films. Biosensor building and ligand detection. Bovine Erythrocyte Membranes (BEM), obtained from cattle blood, were used as an acetylcholinesterase source to form a Langmuir film at the air-water interface. One-layer Langmuir-Blodgett films (LB_{BEM}) were obtained by transferring the BEM monolayer to alkylated glass substrates at a constant π. The catalytic efficiency exhibited a huge increase with BEA in LB_{BEM} compared with BEA in BEM vesicles. Moreover, the supported BEA was able to sense the presence of monoterpenes in the incubation medium, reproducing the previously described inhibition effect.

1. INTRODUCTION

Some membrane-bound proteins are anchored to the plasma membrane through the insertion of a covalently attached lipid moiety, e.g fatty acids, isoprenoids and **g**lyco**p**hosphatidyl**i**nositol (GPI) [1, 2]. In particular, the GPI anchor type directs proteins to the outer hemilayer (extracellular side of the membrane), where they segregate preferentially in microdomains enriched with cholesterol (CHO) and glycosphingolipids [1, 2]. However, the molecular environment of the apoprotein of a GPI-anchored protein is the cell glycocalyx (CG). The latter is defined as a dense matrix of carbohydrate residues covalently linked to glycolipids or to membrane-bound glycoproteins [3]. The CG could be considered as a molecular crowded environment [4] where the conformation and the activity of proteins are conditioned by phenomena such as restrictions in the water availability as a solvent and impairment in the diffusion of solutes as a consequence of the excluded volume. The membrane structure and dynamics involve different hierarchical levels of organization and the protein activity and conformation can be coupled to the membrane dynamics [5, 6]. In turn, the physical membrane properties such as curvature, molecular density, packing defects and thickness are mutually affected within magnitude ranges allowing to satisfy a stable organization of the system [7]. Changes in the membrane molecular density can affect the degree of exposure of integral membrane proteins to the aqueous phase, and thus may affect the access of ligands to their binding sites in the protein. Also, rheological transitions within the GC may accompany the bilayer dynamics [8] with the consequent effects on water structure [9] and diffusional phenomena [10] in these environments.

In the present paper we examine the kinetic behavior of a GPI-anchored enzyme, the Acetylcholinesterase (AChE) from **B**ovine **E**rythrocyte **M**embranes (BEM). The most studied AChE is that located in the synaptic cleft which is involved in the termination of nerve impulses in cholinergic synapses, hydrolyzing the cationic neurotransmitter acetylcholine to choline and acetic acid [11]. However, AChEs exhibit an extensive tissue distribution in mammals [12, 13] and are widely distributed among different species [14]. Interestingly, the presence of AChE of insects and arthropods suggests its potential as a target to develop new kinds of pesticides. These would constitute an environmentally friendly and a profitable alternative to synthetic insecticides such as the well-known toxic organophosphates.

Several results reported in the literature suggest a correlation between the dynamic properties of the membrane and the catalytic activity of the enzyme. Firstly, it has been observed that the denaturation temperature is considerably lower in solubilized **B**ovine **E**rythrocyte **A**cetylcholinesterase (BEA) than in the native, membrane-anchored protein, suggesting that the membrane has a stabilizing effect on the protein structure, even though this enzyme protrudes into the extracellular compartment [15]. Also, the thermal dependence of human BEA activity analyzed through Arrhenius plots (ln K vs. 1/T), exhibited a straight line in the case of the purified enzyme and

a biphasic behavior with a break in the case of the enzyme reconstituted in liposomes, matching with the gel to liquid crystalline phase transition temperature of this phospholipid. These results suggested that the conformational changes of BEA induced by temperature can be modulated by the lipid environment [16, 17]. Moreover, it has been reported that BEA molecules are preferably anchored in the most ordered membrane domains (such as CHO-rich domains) and its activity can be modified by the increase in membrane fluidity through the treatment with *n*-butanol or temperature [15].

The use of phospholipids in self-organized monolayers at the air-water interface, provides a consistent flat topography and a controlled degree of molecular crowding [18-20]. In addition, monolayers can be transferred to functionalized surfaces (both hydrophobic and hydrophilic) to obtain monolayers supported on a flat surface, called Langmuir-Blodgett films (LB), where the molecular organization of the initial floating monolayer is preserved [19-23].

Although model membranes with simple composition allow dissecting the effects of individual variables acting on a given phenomenon, understanding the behavior of complex systems requires, at some point, the restoration of the elements that allow the approach to a real system. Consequently, an intermediate situation between the natural membrane and the LB model with pure lipids, could be the LB constituted by a natural membrane transferred to a solid support [19, 20, 23]. The use of natural membranes as a source of enzyme, not only facilitates the building of biosensors saving time and costs of purification of the enzyme from its source, but also offers compositional and structural complexity allowing the study of various phenomena of biophysical and cellular interest. Being BEA a membrane-bound enzyme with a hydrophobic GPI anchor, allowing the transmission of information between the protein and the interface, it is expected that the kinetics of the BEA catalyzed reaction would be able to report information about the dynamical changes that occur in the enzyme molecular environment.

So, in the present paper we firstly prepared Langmuir films by the spreading of BEM (LF_{BEM}) at the air-water interface and then we transferred LF_{BEM} packed at different constant lateral pressures to alkylated glasses to obtain Langmuir-Blodgett films of BEM (LB_{BEM}). LF_{BEM} and LB_{BEM} films were characterized from the chemical, rheological and topographical viewpoints. Finally, we measured the BEA catalytic activity to characterize the modulation induced by the molecular dynamics of its environment in LB_{BEM} using BEM aqueous suspensions (S_{BEM}) as a reference sample. As a result, we obtained stable LB_{BEM} films where the catalytic efficiency of BEA not only was preserved but also was improved with respect to BEA in S_{BEM}.

Furthermore, in the present work, BEA in LB_{BEM} was used as the reference enzyme to test the effect of two monoterpenes (MTs), eugenol and 1,8-cineol, which have been demonstrated effective at modulating AChE from different species including insects and other arthropods [14]. We observed that in the sub-millimolar range they were able to increase BEA activity and in the millimolar range to inhibit it.

2. MATERIALS AND METHODS

2.1 Materials

Eugenol (2-Methoxy-4-(prop-2-en-1-yl)phenol, MW 164.2) and 1,8-cineol (1,3,3-trimethyl-2-oxabicyclo[2.2.2]octane, MW 154.25) were obtained from a local supplier (Todo Droga) and their purity was checked by Gas Chromatography using a Shimadzu GC-R1A with a flame ionization detector and a DB-5 capillary column (30 m×0.5 mm i.d.) at a N_2 flow rate of 0.9 ml/min. All other reagents were of analytical grade.

2.2 Purification of bovine erythrocytic membranes (BEM)

Blood extracted by puncture from healthy cattle, was preserved at 4°C in extraction bags containing sodium citrate as anticoagulant and monohydrate dextrose. The plasma was eliminated by centrifugation at 1500 x g, for 10 min. The pellet fraction containing the white blood cells ('buffy coat') was aspirated with a Pasteur pipette, and the remaining material was suspended in pH 7.4, isotonic 5 mM phosphate buffer, containing 145.4 mM NaCl and 4.5 mM KCl (phosphate buffer saline, PBS) and filtrated in a 1:1 cellulose/microcrystalline cellulose mixture, to remove completely the white blood cells [24]. The filtrate was centrifuged three times for 10 min at 1500 x g, discarding the supernatant after each centrifugation. In the last centrifugation, carried out at 2500 x g, a pellet of "packed" erythrocytes was resuspended in pH 8, 5 mM hypotonic phosphate buffer, with 0.5 mM EDTA. Successive centrifugations were then performed at 12,500 x g for 40 min until a hemoglobin-free pellet of **b**ovine **e**rythrocyte **m**embranes (BEM) was isolated [25]. BEM were lyophilized and stored at -20 ºC until the time of their use for the experiments, for which they were resuspended in bidistilled water.

2.3 Membrane chemical composition

2.3.1 Protein quantification

Proteins were quantified by the Lowry method [26] modified by Markwell et al. [27] by the addition of SDS in the EDTA-Cu^{2+} reagent. 100 µl of suspension of the different protein fractions were added to 1 ml of the reaction mixture (0.3% w/v SDS in 0.63 mM EDTA Cu^{2+}). In the case of Langmuir-Blodgett (LB) films, they were firstly cut in small pieces, washed with 50 µl of 1% w/v SDS, then 0.5 ml of the reaction medium (0.63 mM EDTA Cu^{2+}) were added and the whole mixture was sonicated for 15 min at 80 W and 40 kHz frequency at room temperature. In all cases, samples were incubated for 30 min at room temperature. Finally, the Folin–Cicalteau reagent was added and the absorbance at 750 nm was measured after another 1 h incubation period.

2.3.2 Phospholipid quantification

Phospholipids were quantified by the Fiske-Subbarow method, modified by Chen [28]. In the case of LB films, the phospholipids adsorbed on the alkylated glass were extracted by sonication of the coverslip in the presence of an SDS aqueous solution (1% w/v) for 15 min. All the samples were submitted to water evaporation by heating at 140°C for 1h. Then, the dry material was treated with 0.2 ml of $HClO_4$ for 60 min at 200 ºC, and the released inorganic phosphate was quantified as indicated above. The phospholipid concentration was inferred from the phosphate concentration, assuming an average phospholipid molecular weight of 700 Da.

2.3.3 Polyacrylamide Gel Electrophoresis (SDS–PAGE)

The electrophoresis was carried out in 10% polyacrylamide gels in the presence of SDS (SDS-PAGE). Mini-gels of 10 cm x 7 cm x 0.75 mm were run in a Mini-Protean III Cell (Bio-Rad) at 100 mV constant voltage. Protein bands were stained with Coomassie Brilliant Blue R-250. The molecular weight markers were myosin, β-galactosidase, phosphorylase B, serum albumin and ovalbumin, with molecular weights 200,000; 116,250; 97,4000; 66,200 and 45,000 Da, respectively.

Two sets of samples were assayed. One of them included the different fractions obtained throughout the BEM purification procedure (blood, "packed" erythrocytes and BEM before and after the filtration through cellulose). The other set of samples consisted of microcellulose filtrated BEM (or BEM components) in the different organizations used afterwards as enzyme sources (full BEM dispersed in distilled water (S_{BEM}); Langmuir films set at 35 mN/m (LF_{BEM}) and Langmuir-Blodgett films transferred at 35 mN/m (LB_{BEM})). LF_{BEM} were collected by aspirating the material spread over the air-water until π dropped to zero. For the extraction of the film transferred to the solid support, the LB_{BEM} were immersed in a 1 % w/v SDS solution and sonicated for 1 min in a sonication bath.

2.4 Langmuir-films from bovine erythrocyte membranes (LF_{BEM})

2.4.1 Langmuir films preparation

LF_{BEM} were prepared and monitored as described previously [19, 20]. An aqueous dispersion of lyophilized BEM was spread over an air-water interface placed in a Teflon trough (230 ml volume) which was enclosed in a Plexiglas box to reduce surface contamination. Before each experiment the trough was rinsed and wiped with 96% v/v ethanol and several times with bidistilled water. The absence of surface-active compounds in pure solvents and in the subphase solution (bidistilled water) was checked before each run by reducing the available surface area to less than 10% of its original value after enough time was allowed for the adsorption of possible impurities that might have been present in trace amounts. Approximately 150 µl of S_{BEM} containing 0.53 mg protein/ml was spread with a syringe directly on the interface at ~10 µl/min rate (Fig. 1a) and at an initial area of 242.25 cm^2. Monolayers were led ~15 min to stabilize before starting the compression.

2.4.2 Surface Pressure-Area and Surface Potential-Area isotherms

Surface pressure (π) and surface potential (*ΔV*) vs. Area (*A*) isotherms were recorded simultaneously, monitored continuously by means of a computer-controlled commercial device (Minitrough II, KSV Instruments Ltd., Finland) while the film was symmetrically compressed at a constant rate of 5 cm^2/min by means of two barriers moving synchronously. The experiments were carried out at 25 ± 1°C. π was measured by the Wilhelmy plate method, using a roughened platinum plate (a platinized Pt foil; 5x20x0.025 mm, length x width x height). ΔV was measured by the vibrating plate method (Spot Tune- KSV ltd.). Given that the characterization level achieved in the lipid and protein composition of BEM was not deep enough to estimate an average molecular area, the isotherms were expressed as a function of the percentage of compression ($C_{\%}$). To analyze more deeply the phase behavior of the films, the compressibility modulus (*K*) was calculated with Eq.1, being A the trough area in cm^2 and π the surface pressure in mN/m.

$$K = -A\left(\frac{d\pi}{dA}\right)_T \quad [1]$$

2.4.3 Monolayer stability and thermodynamic analysis

LF_{BEM} were submitted to three successive compression– decompression (C–D) isocycles. Two series of experiments were carried out from the same initial π = 0 mN/m, each one differing in the final π reached at the first compression (12 mN/m or 40 mN/m, values respectively far from or close to the collapse pressure, π_c, of the monolayer). LF_{BEM} were decompressed up to the initial area, in both cases. *K vs. A* plots were also calculated for each cycle and plotted vs. the percentage of compression.

The C-D free energies of compression (ΔG_C) and decompression (ΔG_D) were calculated as the area beneath the *π–A* isotherm:

$$\Delta G_C = \int_0^{\pi_c} A_{BEM}\,\delta\pi \quad [2]$$

$$\Delta G_D = \int_{\pi_c}^{0} A_{BEM}\,\delta\pi \quad [3]$$

The $\Delta\Delta G = \Delta G_C - \Delta G_D$ allowed to evaluate the occurrence of hysteresis throughout C–D cycles.

2.5 Langmuir-Blodgett Films from bovine erythrocyte membranes (LB_{BEM})

LB_{BEM} were prepared at two different lateral pressures, 10 mN/m ($LB_{BEM,10}$) and 35 mN/m ($LB_{BEM,35}$) by the transfer of LF_{BEM} onto chemically modified microscopy glass-coverslips, 12 mm diameter and 0.15 mm thickness. This modification (alkylation) consists of the chemical reaction between the silicate groups of the glass and an alkyl trichlorosilane group which is attached to a 18-carbon chain, following the procedure described by von Tscharner and McConnell [29].

Langmuir films were prepared, and after the π stabilization, an alkylated glass was immersed in the subphase perpendicularly to the interface. The monolayer was transferred on both sides of the silanized glass (see Fig. 1b). In order to maintain a constant π throughout the transference, a

continuous movement of the barrier compensated the π fall due to the loss of monolayer from the air–water interface. The transfer ratio (TR) was calculated as the relationship between the reduction in the monolayer area and the total glass area. Several alkylated glasses covered with LB_{BEM} films on both sides could be obtained from a single monolayer, which were received in a 24-well plate immersed in the subphase. LB_{BEM} were stored underwater and at 4° C until further use (not more than 48 hours later, except in the stability assays).

2.6 Topographic characterization of Langmuir and Langmuir-Blodgett films

2.6.1 Epifluorescence Microscopy (EFM)

The bidimensional structure of LF_{BEM} and LB_{BEM} was studied by epifluorescence microscopy (EFM). A KSV Minisystems surface barostat was mounted on the stage of a Nikon Eclipse TE2000-U (Tokyo, Japan) microscope, with a color video camera Nikon DS-5 M with a supported resolution up to 2,560–1,920 pix (Capture) and a long-distance 20x objective. BEM were doped with 0.5 mol% of 1,1'-Dioctadecyl-3,3,3',3'-Tetramethylindotricarbocyanine Iodide (DiI-C18). LF_{BEM} were observed *in-situ* and, as well as LB_{BEM}, were observed from below.

2.6.2 Brewster angle microscopy (BAM)

LF_{BEM} were prepared over an aqueous subphase, as described above. The Langmuir trough was mounted on the stage of a Brewster angle microscope (BAM) coupled to an EP3 Imaging Ellipsometer equipment (Accurion, Goettingen, Germany) with a 20x objective (Nikon, Japan, NA 0.35). Minimum reflection was set with a polarized 532λ laser incident on the bare aqueous surfaces at the experimentally calibrated Brewster angle (~53.1°). For image acquisition, the LF_{BEM} was compressed until reaching the desired lateral pressure, the compression was stopped at this lateral packing, and 3–5 images were taken. The gray level at selected regions of the BAM images were obtained from the software ImageJ 1.51q [30] and the reflectivity values were calculated considering the calibration factors for each individual experiment [31]. The reflectivity obtained from BAM measurements is directly related to the square of the film thickness and to the refraction index of the film [31].

2.6.3 Atomic force microscopy (AFM)

For atomic force microscopy (AFM) imaging of LB_{BEM} a Bruker INNOVA microscope was used with the following settings: tapping mode, 0.12 Hz scan frequency, drive amplitude 0.12V, Gain x8, phase 5.78º. The cantilever was a 600 nm silicon tip on nitride lever. Sweep parameters: time 1000 sec, resolution 0.0059 kHz, phase 6º. The topographic structure of the microscopic images was studied with the NanoScope Analysis v140r1sr2 free software.

2.7 Determination of BEA enzymatic activity

The catalytic activity of BEA was measured as a function of time, protein concentration and substrate concentration according to the spectrophotometric method of Ellman et al [32]. Briefly, the hydrolysis of acetylthiocholine (a substrate analog) catalyzed by BEA in 0.1 M, pH 8 phosphate buffer at 37 ºC, produced thiocholine and acetate. This was coupled with the reaction of the thiocholine with the dithiobisnitrobenzoate ion (DTNB). The final product has an extinction molar coefficient at 412 nm ε_{412} = 13.600 M^{-1} cm^{-1}. The incubation system consisted of 9 μl of DTNB (2mM), 40 μl of a 1:60 dilution of the S_{BEM} sample (0.28 mg/ml protein), in the presence of the substrate, in a final volume of 220 μl.

When the enzyme source were LB_{BEM} films, the covered glasses were immersed in 2,200 µl final volume maintaining the same proportion of the previous incubation medium, see Fig. 1c. It should be recalled that the LB_{BEM} covered glasses were received in a 24-wells plate in the subphase underneath the monolayer (section 2.5) (Fig. 1b). The remaining monolayer and the subphase were eliminated by aspiration. The LB_{BEM} films, without being removed from the multi-well plate, were washed several times with 0.1 M pH 8 phosphate buffer to replace the original subphase. So, the LB_{BEM} were never exposed to the air.

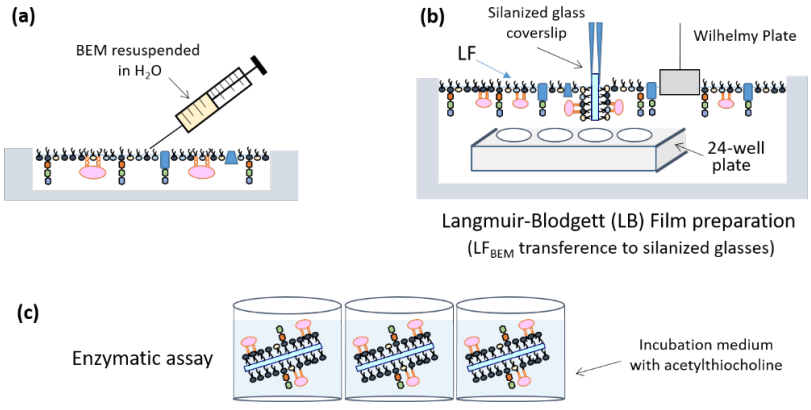

Figure 1. Schematic representation of (a) BEM spreading over the air-water interface to form the LF_{BEM}, (b) transference process of LF_{BEM} from the air-water interface to the alkylated glass to obtain LB_{BEM} films and (c) BEA catalytic activity assays using LB_{BEM} films as the enzyme source.

The assays were performed as independent triplicates for each substrate concentration point. The absence of non-enzymatic hydrolysis was verified in the presence of silanized glass free of LB_{BEM}.

V_{max} (maximal reaction rate) and K_M (Michaelis-Menten constant) parameters resulted from the Michaelis–Menten equation (Eq.4) fitted to the plot of the initial reaction rate (V_0) vs. the substrate (S) concentration.

$$V_0 - \frac{V_{max} \cdot S}{K_M + S} \qquad [4]$$

V_0 was defined as the amount of product (thiocholine), obtained in conditions of optimal incubation time and enzyme concentration, per time unit per amount of total protein. It was expressed as nmole of product/min/µg protein.

Optimal conditions for the incubation time (t_0) in S_{BEM} (Fig.S1) and LB_{BEM} (Fig.S2) and protein concentration ($[Protein]_0$) in S_{BEM} (Fig.S3) were determined in separate experiments. The activity of BEA in LB_{BEM} was tested at a single protein concentration since the amount of BEA in these samples is related to the BEM present in the LF_{BEM} transferred to the alkylated glass. In the experiments to determine the kinetic parameters K_M and V_{max}, the substrate concentration varied between 0 (blank) and 0.6 mM. The catalytic stability of the film was evaluated at 1, 2, 4, 7 and 14 days from the transference of the LF_{BEM}, packed at 10 or 35 mN/m, to the alkylated glass substrate. The films were built and kept under water at 4ºC until their use. The enzymatic activity was evaluated at 0.4 mM final substrate concentration.

BEA activity in LB_{BEM} was also tested in the presence of two monoterpenes (1,8-cineol and eugenol) at 0.01, 0.1 and 1 mg/mL (~0.06, ~0.6 and ~6 mM, respectively) final concentrations at 0.4 mM fixed substrate concentration. The effect was defined as the percentage of activity with respect to the control without monoterpene. All determinations were performed in triplicates.

2.8 Statistical Calculations

The least squares method was applied to fit functions through a nonlinear regression analysis. Student's t test was applied to compare individual averages. The propagation error method was used to evaluate the error associated with variables calculated from other ones determined experimentally. ANOVA and Duncan post-hoc tests were applied for comparisons with Prism v.6.01 software (GraphPad Software, Inc.). s.e.m., standard error of the mean; d.f., degrees of freedom.

Biochimica et Biophysica Acta (BBA) - Biomembranes.
Volume 1862, Issue 5, 1 May 2020, 183188
https://doi.org/10.1016/j.bbamem.2020.183188

3. RESULTS AND DISCUSSION

3.1 Protein composition of bovine erythrocyte membrane fractions

Electrophoresis was conducted under denaturing conditions, using the fractions obtained from the different steps throughout the purification protocol of BEM. In the literature, this fraction is also referred to as erythrocyte "ghost", since they comprise the cell plasma membrane free from cytoplasmic content after the lysis through a hypo-osmotic shock.

Fig. 2 depicts the band pattern and the corresponding densitometric profiles. It can be observed that plasmatic proteins, such as albumin (66.2 kDa), which are stained with high intensity in the lane corresponding to full blood (Fig. 2b) are absent in the BEM fraction (Figs. 2d and 2e). Moreover, bands typically associated with proteins from white blood cells, included within the clasp in Fig. 2d, do not appear in BEM after filtration (Fig. 2e).

Also, a couple of bands that were barely detected in the unfiltered BEM sample were enriched after filtration (Fig. 2e, black arrows).

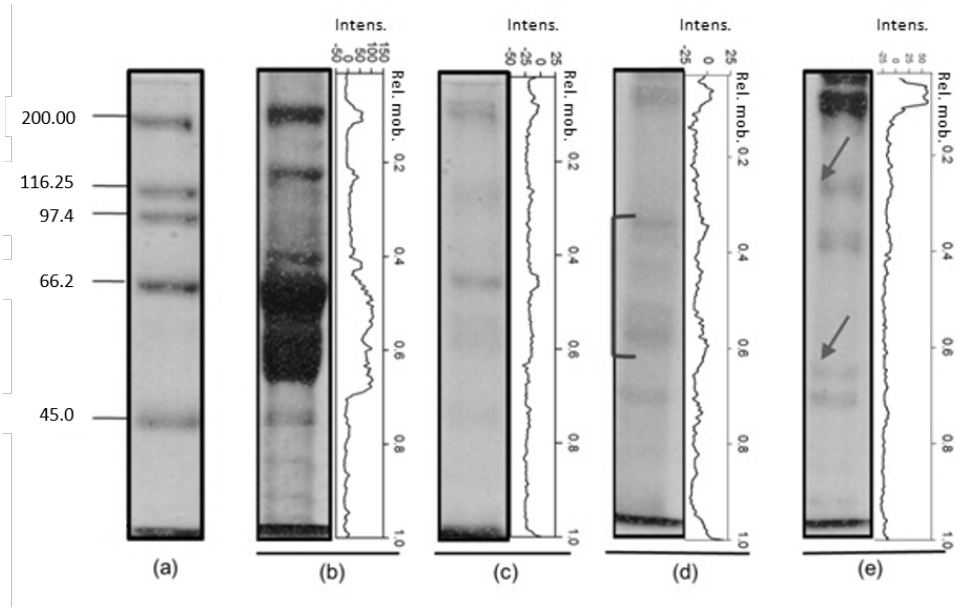

Figure 2. SDS - 10% PAGE of the different fractions obtained along BEM purification. Proteins were stained with Coomasie Blue R-250. (a) Molecular weight markers (MWM); (b) blood; (c) "packed" erythrocytes; (d) BEM before filtering; (e) BEM after filtration. Densitometric profiles of the protein bands are shown at the right of each electrophoretic image. The clasp includes a set of proteins that belong to white blood cells. Gray arrows point to erythrocytic proteins enriched in the BEM fraction obtained after the filtration process.

The protein composition upon LF_{BEM} formation was almost unaffected if compared with BEM suspension (Fig. 3, S_{BEM} and $LF_{BEM,35}$ lanes) in spite of the stress suffered by BEM vesicles when they were spread over the air-water interface and suffered a bilayer to monolayer transformation. However, the loss of some low molecular weight proteins occurred during the transference of LF_{BEM} to the

alkylated glass to form the LB_{BEM} (compare lanes $LF_{BEM,35}$ and $LB_{BEM,35}$ in Fig.3). The expected location of the BEA monomer (MW = 77 kDa), pointed to by the arrow and lines in Fig.3, seemed to be preserved during these processes.

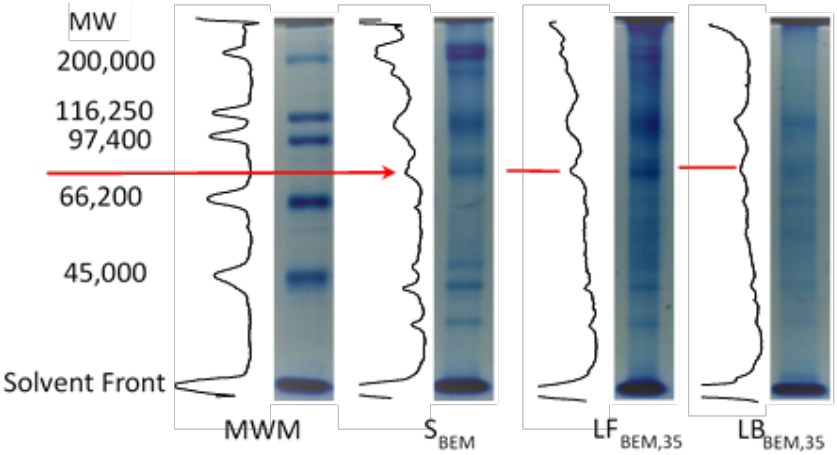

Figure 3. SDS – 10% PAGE comparing the change in protein composition from a BEM suspension to $LF_{BEM,35}$ and $LB_{BEM,35}$ films. MWM, molecular weight markers; S_{BEM}, suspension of bovine erythrocyte membranes; $LF_{BEM,35}$, Langmuir film collected from the air-water interface, previously packed at 35 mN/m; $LB_{BEM,35}$, Langmuir film transferred at 35 mN/m to the alkylated glass. Each lane is accompanied by its densitometric profile. Red arrow and red lines indicate the expected position of the BEA monomer, according to its molecular weight. Coomasie Blue R-250 staining.

3.2 *Langmuir films from bovine erythrocytic membranes (LF_{BEM})*

3.2.1 Rheologic behavior

Stable monolayers were formed from the spreading of S_{BEM} at the air-water interface. The compression π-A and the surface potential vs. area (ΔV-A) isotherms were measured experimentally and recorded simultaneously. As stated in section 2.4.2, the isotherms are shown as a function of the percentage of compression ($C_{\%}$). It was calculated considering the initial trough area as 0% and the end of the compression as the 100%. The compressional modulus (K) vs. A isotherm was calculated from Eq.1 (Fig. 4) and is also plotted as a function of $C_{\%}$.

In the isothermal compression, the LF_{BEM} reached a molecular coherence at the lift-off point, marked by the departure of π from zero, and the closest molecular packing at π_c. In the π-$C_{\%}$ isotherm, three main two-dimensional (2D) transitions were observed (marked as t_1, t_2 and t_3, from the lowest to the highest π). The transitions were clearly evidenced as inflection points in the K-$C_{\%}$ isotherms, beginning at a maximum and continuing with an abrupt slope decrease in the K-$C_{\%}$ plot. The values pointed to in Fig. 4 correspond to π values at mid-transition points. The presence of these transitions evidenced the complex nature of LF_{BEM}, which comes from a biomembrane composed approximately

of 50% protein by weight. The values of K at the π_c and at the different transition midpoints (π_t), indicate that LF_{BEM}, at the temperature of the present assays, exhibits a liquid expanded behavior throughout the whole isotherm [33, 34].

The surface potential (ΔV) reflects the resultant, in the direction perpendicular to the interface, of the density and the orientation of all the molecular dipoles in the sample where the polar moieties orient towards the water and the hydrophobic groups towards the air [35].

Before the beginning of the compression, immediately after S_{BEM} spreading, the ΔV exhibited a non-zero value (~0.26 V). Then, upon the compression progressed, ΔV began to increase even before the $\pi_{lift\text{-}off}$. This indicates that ΔV is more sensitive than π to detect the presence of surfactants and their molecular dipoles over the air-water interface which affect the electric field before the formation of a coherent film. The t_1 was evidenced in the ΔV-A plot as a sudden increase in ΔV (gray line, Fig. 4) which, analyzed in conjunction with K, clearly reflects a dramatic interfacial molecular reorganization, increasing the film elasticity afterwards this transition, contrary to what would be expected if the film were composed of pure lipids. Similar 2D-transitions have been associated with protein reorganization at the interface for other natural membranes [19, 36, 37] and have also been observed in monolayers of lipid grafted polymers [38]. After t_1, the ΔV increases gradually until the collapse of the monolayer. t_2 and t_3 where slightly evidenced in ΔV plot profile, which reflects the absence of significant molecular dipole reorganizations.

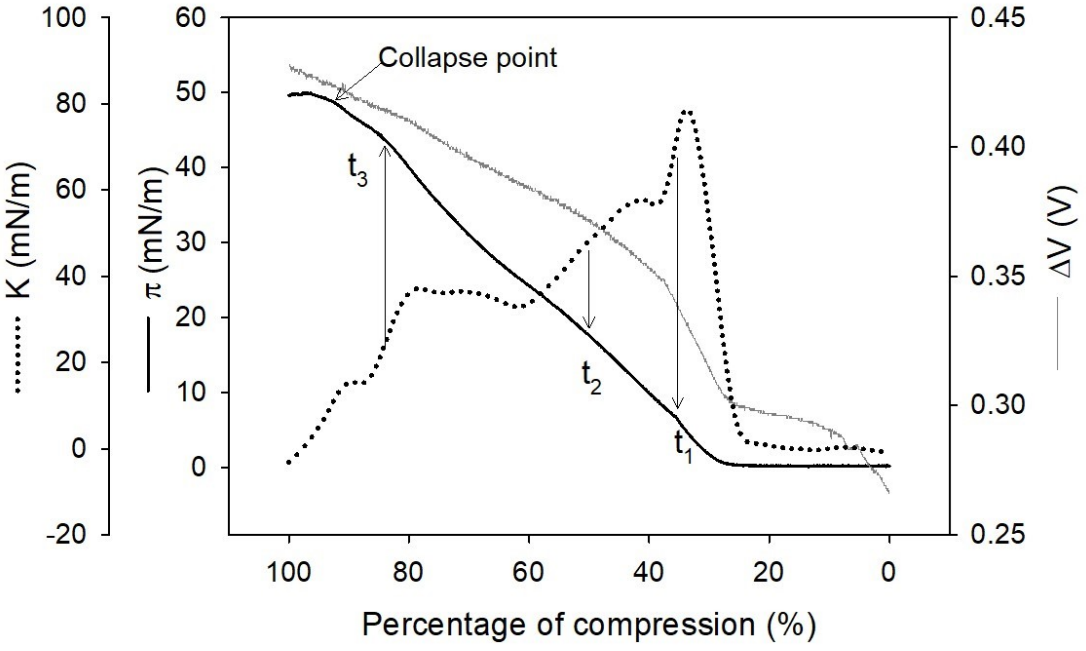

Figure 4. Surface pressure (π), compressional modulus (K) and surface potential (ΔV) vs. percentage of compression ($C_{\%}$) isotherms of BEM at the air-water interface.

The behavior of BEM monolayer was reproducible, and the values of the molecular parameters obtained are synthesized in Table 1.

Table 1 Molecular parameters derived from π-C%, ΔV-C% and K-C% compression isotherms.

Parameter	Parameter values			
	Transitions midpoints			Collapse point
	π_{t1}	π_{t2}	π_{t3}	π_C
π (mN/m)	7.73 ± 0.53	17.76 ± 0.19	43.05 ± 0.12	49.08 ± 0.12
K (mN/m)	72.25 ± 4.8	51.26 ± 2.1	28.32 ± 1.22	5.25 ± 1.3
ΔV (V)	0.352 ± 0.006	0.372 ± 0.006	0.414 ± 0.007	0.428 ± 0.006

Numbers are the mean ± s.e.m of triplicates determined from independent isotherms. π_c, collapse point; π_{ti}, surface pressure value at the midpoint of the i^{th} 2D-transition identified from the evolution of the K- $C_{\%}$ isotherm. $C_{\%}$, percentage of compression.

3.2.2 Compression-Decompression cycles (CD)

The film stability was evaluated under successive CD cycles within the same area range (Fig.5). The compressional modulus (K) was calculated against the trough area (A) and plotted as a function of the percentage of compression ($C_{\%}$)**.** Starting at π≅0 mN/m, the monolayers were compressed either up to 12±2 mN/m (before the main transition) named as $CD_{0\text{-}12\text{-}0}$ (Figs.5a-5d), or up to 40 mN/m ($CD_{0\text{-}40\text{-}0}$), before the collapse point to avoid the film destabilization (Figs.5e-5h).

Biochimica et Biophysica Acta (BBA) - Biomembranes.
Volume 1862, Issue 5, 1 May 2020, 183188
https://doi.org/10.1016/j.bbamem.2020.183188

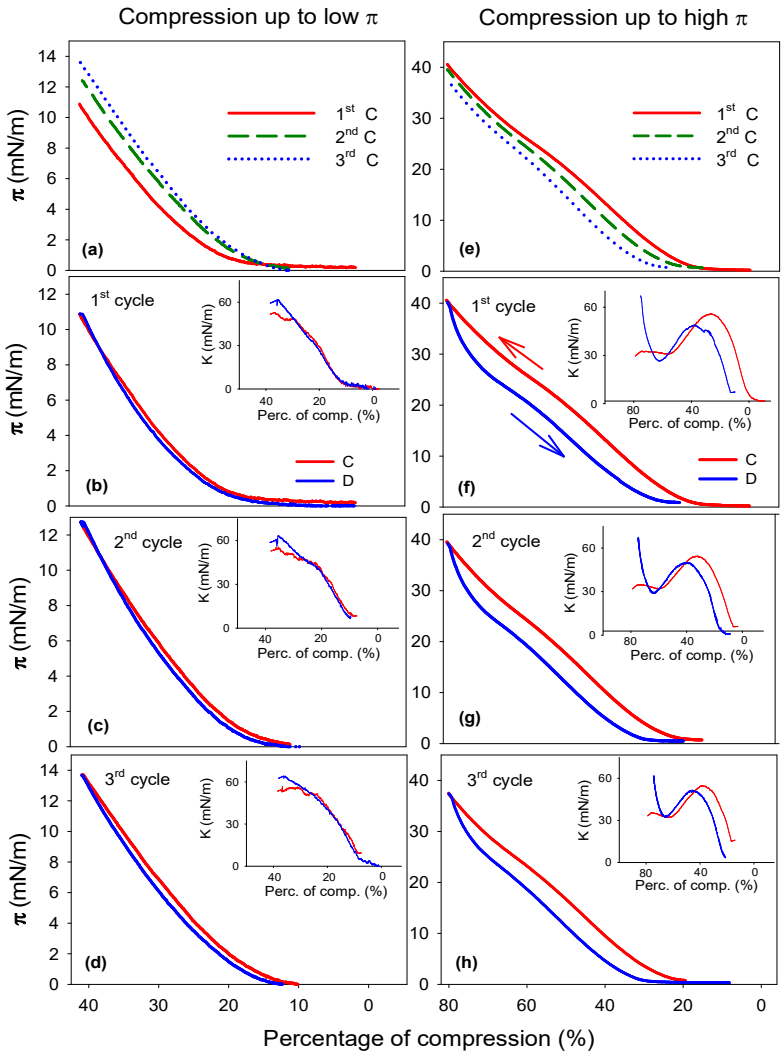

Figure 5. Behavior of LF$_{BEM}$ along Compression-Decompression cycles. The cycles were analyzed up to a maximal π = 12 mN/m (a-d) or up to π = 40 mN/m (e-h). In (a) and (e) the three compression isotherms are shown in the same panel for an easy comparison. Compression plus decompression isotherms of each of the successive cycles are shown separately (b-d and f-h) with their respective K vs. C$_{\%}$ graph as insets. The arrows in (f) indicates the direction of the compression (red lines) and that of the decompression (blue lines).

The 0-12-0 mN/m cycles (CD$_{0\text{-}12\text{-}0}$) exhibited a superposition between the C and D in π-C% (Figs.5a-5d) and K-C$_{\%}$ isotherms (Figs.5a-5d, insets). The results reflected a stable BEM monolayer that evidenced a reversible behavior within each C-D$_{0\text{-}12\text{-}0}$ cycle. However, from the 1st to the 3rd cycle a small increase in the slope of the isotherms are observed, increasing either the maximum K (52.7, 54.7 and 56.8 mN/m,) and the maximum π reached (10.9, 12.4. and 13.7 mN/m) along the successive CD cycles (Table 2). This behavior probably shows the loss of some compressible monolayer components during C. In contrast, an expansion of the monolayer (C$_{\%}$ increase) is observed between cycles, ($\pi_{lift\text{-}off}$ of each successive C occurred at bigger C$_{\%}$). We postulate two possible explanations for this behavior, an incorporation of new material incoming from the subphase or an irreversible protein

unfolding. In contrast, when the compression reached a $\pi \sim 40$ mN/m, $CD_{0\text{-}40\text{-}0}$ (Figs.5e-5h), the isotherms between successive cycles showed a displacement towards lower C% values (Figs.5e), implying either material loss towards the aqueous subphase or inelastic compaction of the monolayer components. Also, within each cycle, the D isotherm returned to the initial area at the lowest π when compared with the C isotherm and exhibited lower K at the maximum of the K-$C_{\%}$ plot (Kmax) (Table 2).

Table 2 Maximal compressional modulus (K_{max}) reached during compression and free energy accumulated ($\Delta\Delta G$) in LF_{BEM} after along successive compression-decompression cycles between 0-12 and 0-40 mN/m surface pressures.

C-D cycle	Target surface pressure		Target surface pressure	
	12 ± 2 mN/m	40 mN/m	12 ± 2 mN/m	40 mN/m
	K_{max} (mN/m)		Accumulated free energy ($\Delta\Delta G$) (μJ)	
1st	52.7	55.9	1.8	17
2nd	54.7	54.1	1.7	19
3rd	56.8	54.6	0.9	20

K_{max}, the K value at the maximum in the K-$C_{\%}$ compression isotherm. $\Delta\Delta G$ was calculated as the difference $\Delta\Delta G = [\Delta G_D - \Delta G_C]$ for each C-D cycle, from 0 mN/m to the indicated final surface pressure reached.

The monolayer remains stable within the $CD_{0\text{-}40\text{-}0}$ cycle. From the 1st to the 3rd decompression, the isotherms exhibited a marked hysteresis. This indicates that, in contrast to $CD_{0\text{-}12\text{-}0}$, when high π are reached, the molecular interactions established are not totally reversible and/or the compressed states relax at rates slower than the movement of the barriers, showing that the main transition observed is needed to be trespassed for the hysteresis to occur. A slight displacement of isotherms towards lower $C_{\%}$ along successive $CD_{0\text{-}40\text{-}0}$ cycles might be ascribed to a monolayer leak from the interface towards the subphase and not to the loss of particular components. This is because no significant changes were observed neither in the maximal K achieved (Table 2) nor in the isothermal shape, and no change in the composition of the monolayer was evident.

The magnitude of the energy accumulated in each CD cycle ($\Delta\Delta G_{CD}$) could be calculated taking the free energy of compression (ΔG_C) and subtracting the free energy of decompression (ΔG_D). The $\Delta\Delta G_{CD}$ was also calculated to evaluate the reversibility of the processes (Table 2). $\Delta\Delta G_{CD} \neq 0$ implied irreversibility. The differences in the intermolecular interactions established at low and high π are also reflected in the values of $\Delta\Delta G$ where $\Delta\Delta G_{0\text{-}40\text{-}0}$ resulted in an order of magnitude larger than the $\Delta\Delta G_{0\text{-}12\text{-}0}$ cycles.

3.2.3 Topographic characterization of Langmuir films of BEM (LF_{BEM})

Fig. 6 shows epifluorescence microscopy (EFM) and Brewster angle microscopy (BAM) images of LF_{BEM} which were taken along the compression isotherm at several π values.

3.2.3.1 Epifluorescence microscopy (EFM)

The marked heterogeneity observed by EFM (Figs.6a-6g) and by BAM (Fig.6a'-6g') in the topography of the interface is related to the large number and diversity of lipids and proteins coming from the natural membrane BEM (Fig. 3). Since the analysis of K values are compatible with a monolayer with an expanded behavior throughout the entire isotherm, the coexisting phases evidenced in the EFM micrographs are expected to be in a fluid organization. It is known that the fluorescent probe DiI-C18 is preferentially partitioned into the most ordered phases [39]. Therefore, the areas of the micrographs that exhibit the highest fluorescence intensity could be assumed as a liquid-ordered (Lo) phase

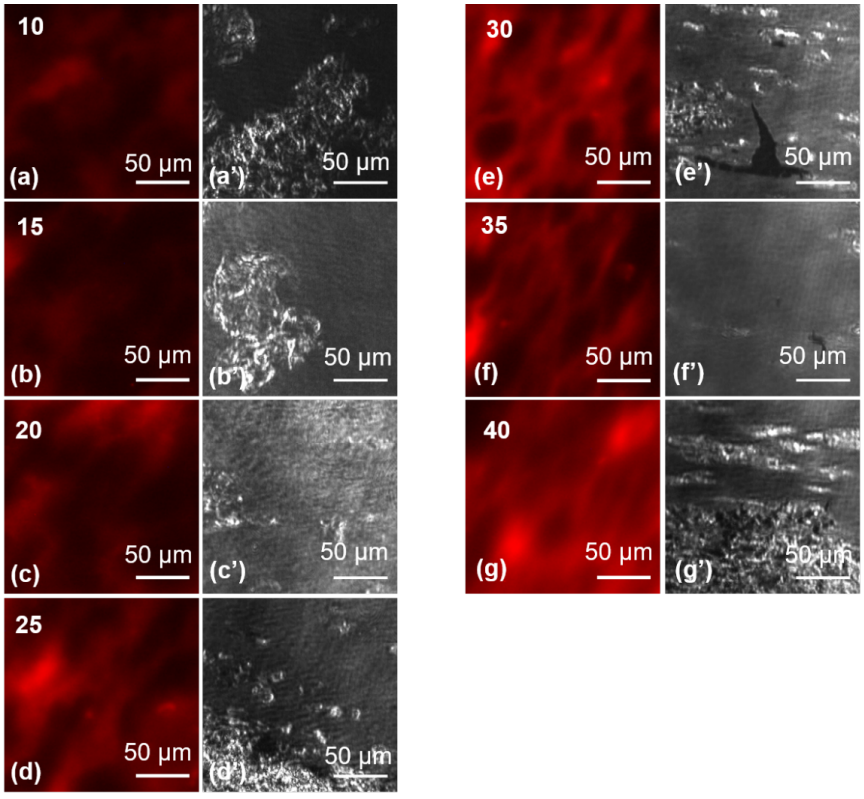

Figure 6. Epifluorescence (EFM) and Brewster angle (BAM) microscopies images of LF_{BEM} at different π. At each π, left and right images correspond to EFM (a-g) and BAM (a'-g'), respectively, at the same π, but from different monolayers. Numbers at the left corners in EFM refer to the corresponding π in mN/m. White bars represent 50 μm. For EFM, the fluorescent dye DiI-C18 was added to the membrane suspension at a 0.5 mol% ratio with respect to phospholipids. All BAM images were captured with calibrated conditions in order to obtain the respective reflectivity. However, the brightness intensity of the BAM images shown were modified so that the background can be resolved.

For this reason, as the compression proceeds, an increase in the proportion of the bright phase (Lo) is observed. Some spots exhibiting a marked fluorescent intensity can be identified as BEM vesicles which remained not spread and attached at the monolayer. Although longer time periods between the deposition of the BEM suspension on the water surface and the start of the compression or successive compression – decompression cycles could have improved the efficiency of BEM spreading, this would have also favored the unfolding of proteins at the interface [40] with negative consequences on the catalytic properties of the enzymes. Moreover, the reproducibility of the π-compression isotherm along 3 C-D cycles supports the stability of the film at the interface and its behavior as a monolayer.

3.2.3.2. Brewster angle microscopy (BAM)

BAM showed highly bright structures of varied sizes and a fractal aspect heterogeneously distributed over a quite homogeneous darker background (Fig.6). This pattern, already described in myelin monolayers [41] was maintained throughout the π range analyzed. The background exhibited a mean reflectivity which increased continuously vs. surface pressure (π) (Figs.7a and 7d) suggesting that the Langmuir film remained at the interface within the π range analyzed. In turn, the bright structures resulted quite incompressible considering the almost constant mean reflectivity determined as a function of π (Fig.7b and 7d). At π≥ 30 mN/m irregular dark regions with reflectivity values similar to that of the air-water interface resembled the presence of cracks in a solid-like film (Fig.7c). This kind of structures were observed in BAM images of myelin monolayers and received a similar interpretation [41].

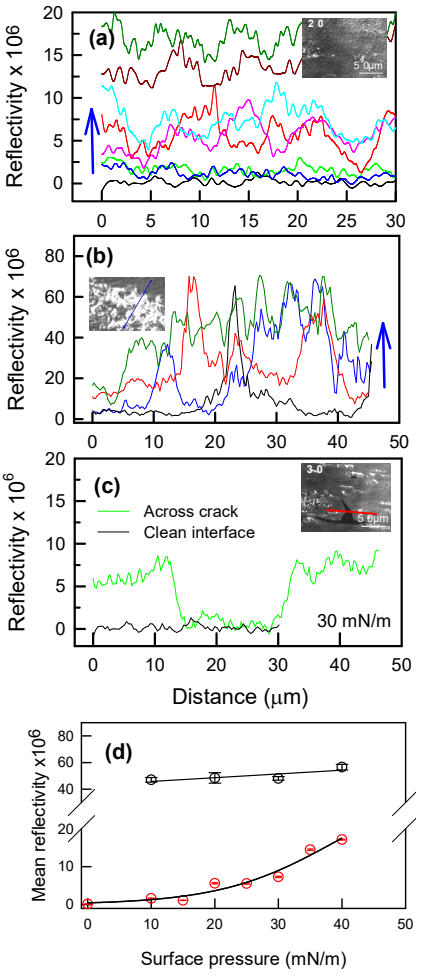

Fig 7. Effect of compression on the reflectivity LF evaluated from BAM images of LF_{BEM}. **(a)** Mean reflectivity profiles of the background within a π-range 0-40 mN/m every 5 mN/m and **(b)** of irregular brilliant structures within 10-40 mN/m every 10 mN/m**. (c)** Reflectivity profiles of the clean air-water interface (—) and of a LF_{BEM} at 30 mN/m along a transect across an irregular dark regions resembling a crack in a solid like film (—). **(d)** Mean ± s.e.m. of reflectivity calculated from the profiles shown in (a) (○) and (b) (○). Blue arrows in (a) and (b) point to the direction of increasing surface pressure.

Biochimica et Biophysica Acta (BBA) - Biomembranes.
Volume 1862, Issue 5, 1 May 2020, 183188
https://doi.org/10.1016/j.bbamem.2020.183188

3.3 Langmuir-Blodgett films (LB_{BEM}) obtained from LF_{BEM}.

3.3.1 Tracing the LF_{BEM} transference and imaging the LB_{BEM} obtained by EFM.

The progression and the quality of the transference of the monolayer from the air-water interface to the solid substrate can be followed by the evolution of two parameters, the Transference (*Tr*) and the cumulative transference (*CT*) (Fig.8a). *Tr* represents the movement of the barriers. *CT* arises from the ratio between the area compensated by the movement of the barriers to maintain a constant π by the area of the solid support that has been submerged at each moment. The result was indicative of a good transference quality since values close to the unity were obtained soon after the start of the process and they were maintained throughout the progression of the transference process.

The transference of LF_{BEM} from the air-water interface to the alkylated glass was performed at two different π, one of them below (10 mN/m) and the other one (35 mN/m) above the t_2 2D-transition revealed in the π-$C_{\%}$ isotherms. The LB_{BEM} were submitted to EFM for its topographical characterization (Fig.8b and 8c). EFM images of LB_{BEM} roughly conserved the topography of the LF_{BEM} they came from.

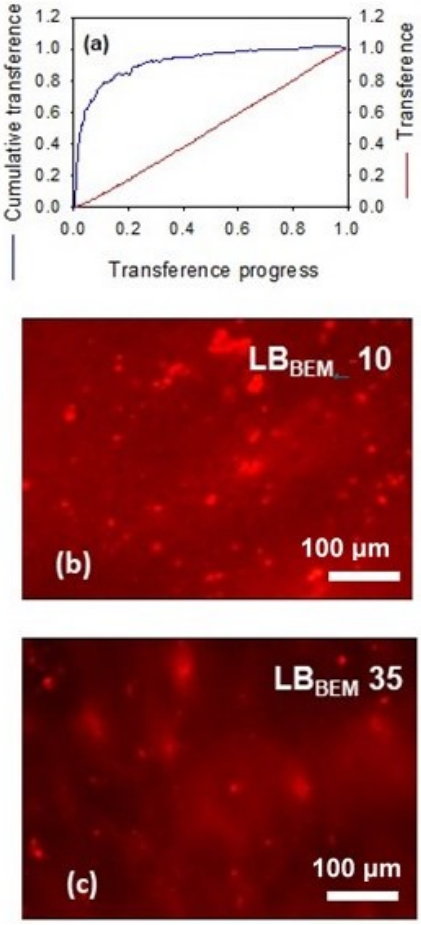

Figure 8. Langmuir-Blodgett films preparation and imaging through epifluorescence microscopy (EFM).
(a) Progression of a typical LF_{BEM} transference process to a solid substrate. The transference progresses from 0 (start stage) to 1 (final stage, reached when the whole solid substrate has crossed the monolayer).
(b) EFM images of the $LB_{BEM,10}$ and $LB_{BEM,35}$ coming from the transference of LF_{BEM} compressed at 10 mN/m or (c) 35 mN/m.
The fluorescent dye DiI-C18 was added to the membrane suspension in a 0.5 mol% ratio with respect to the phospholipids. Experiments were repeated twice with similar results. White bars represent 100 µm.

The resolution of the images captured from LB_{BEM} is better than that obtained with LF_{BEM} probably due to the fact that the former are almost fixed to the substrate while the latters are subjected to the Brownian motion of the water surface and to the air currents of the environment. The $LB_{BEM,35}$ exhibited bright structures with a surface density and definition significantly lower than the $LB_{BEM,10}$. These formations might be non-spread BEM vesicles or may correspond to the fractal low compressible structures resolved by BAM. A similar behavior has already been observed with LB films from other natural membranes [19]. To elucidate this question, we performed AFM imaging of the LB_{BEM}.

3.3.2 Atomic force microscopy of LB_{BEM}

The AFM image of a silanized glass free from LB_{BEM}, exhibits a fine dotted background with a few big bright structures that might be dust particles (Fig. 9a) and a rough background (see height profile at the right, taken along the transect drawn in the picture, Fig.9d). In $LB_{BEM,10}$ image (Fig. 9b) there are some structures of less than 60 nm in height (Fig. 9e), which resemble closed vesicles. However, most of the surface is free of this kind of structures. In Fig. 9c the AFM image of a $LB_{BEM,35}$ exhibits a ~4μm wide depressed region of ~5-10 nm depth (Fig. 9f) which might be a fluid domain. The light brown dots covering the region out of the depression have less than 20 nm in height (Fig. 9g). Considering the size, these dots might be consistent with SUVs (small unilamellar vesicles). However, this is improbable since it is known that SUVs are very stressed structures that require sonication to be obtained.

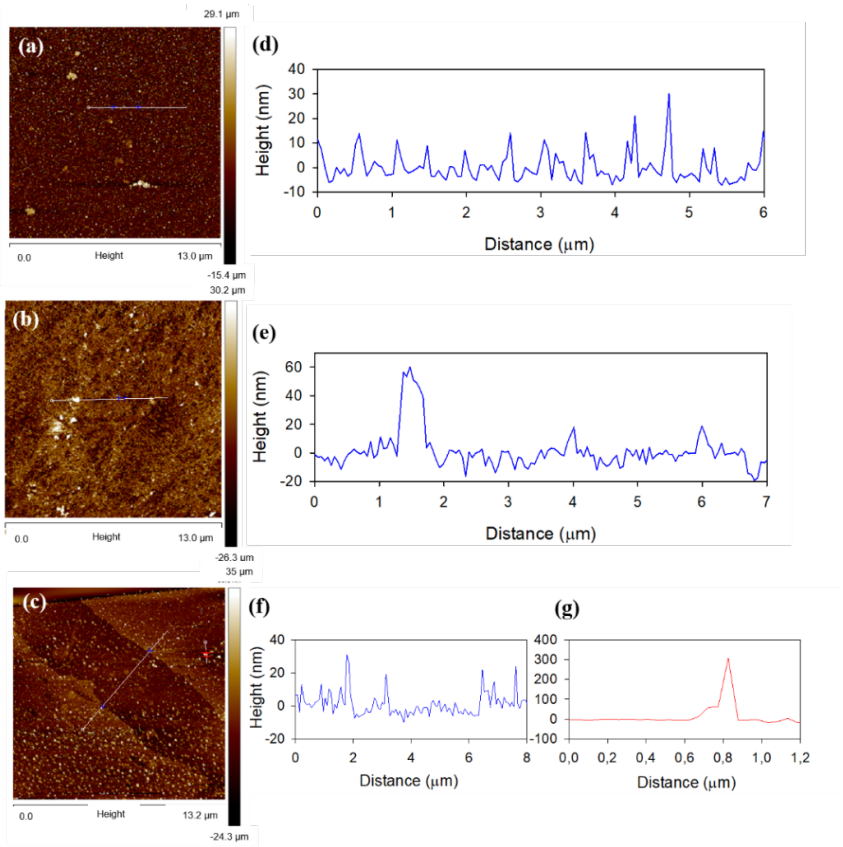

Figure 9. Atomic force microscopy (AFM) images of LB_{BEM}. (a) Alkylated glass free of BEM, (b) $LB_{BEM,10}$ 24 h after the transference, (c) $LB_{BEM,35}$ 24 h after the transference. The image sizes are 13x13 μm. (d-g) Section analysis obtained from AFM images. Each profile corresponds to the image on the left. In the case of $LB_{BEM,35}$ the plot in (f) corresponds to the profile of the white line with blue marks in the AFM image, while the red plot in (g) corresponds to the profile of the white line with red marks.

So, the light brown dots may be some kind of molecular aggregates. On the other hand, the bright white structures, according to their size (300 nm in height and ~1μm wide) (Fig. 9 g) may be taken as vesicles. However, their irregular form suggests the possibility that they may be dust particles as those seen in the first picture of the LB_{BEM}-free silanized glass.

Taken together EFM, BAM and AFM images and the stability of the film after 3 C-D cycles, we can suggest that over the air-water interface as well as over the silanized glass substrate the surface is mostly covered by a monolayer with a few particles dispersed. The latter might be BEM vesicles that remained closed or other kind of molecular structures that segregated from the monolayer phase.

3.4 Kinetics of BEA catalyzed acetylthiocholine hydrolysis

At the experimental conditions of this work, the reactions catalyzed by BEA either in a membrane suspension (S_{BEM}) (Fig. 10a), $LB_{BEM,10}$ (Fig. 10b) or $LB_{BEM,35}$ (Fig. 10c) exhibited a

michaelian (hyperbolic) behavior. Therefore, the kinetic parameters K_M and V_{max} (Table 3) could be calculated by fitting the Michaelis-Menten equation (Eq.2) to the experimental data. The value of K_M measured with S_{BEM} (Table 3) was similar to that reported previously [32].

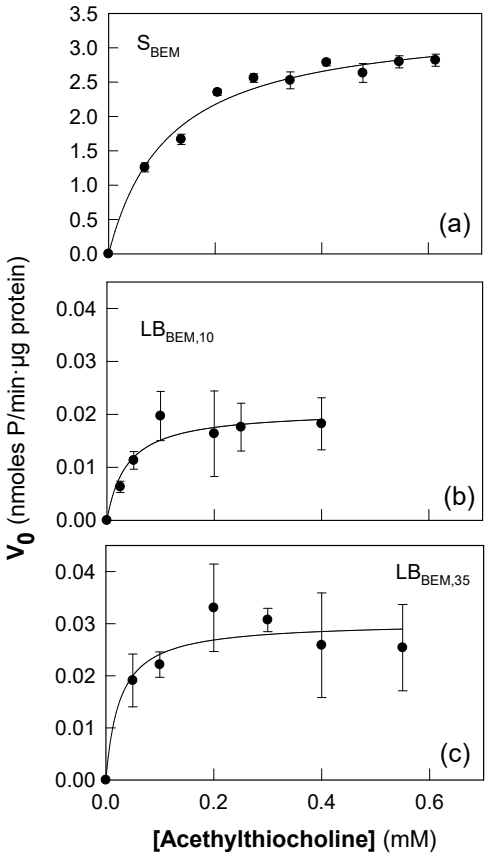

Figure 10. BEA catalytic activity vs. substrate (acetylthiocholine) concentration. Different enzyme sources were used. (a) BEM in suspension (S_{BEM}), (b) $LB_{BEM,10}$; (c) $L_{BBEM,35}$.

3.4.1 Vmax values in Langmuir films transferred to alkylated glasses ($LB_{BEM,10}$ and $LB_{BEM,35}$)

The V_{max} measured with $LB_{BEM,10}$ and $LB_{BEM,35}$ films were considerably lower than that obtained with S_{BEM}. This result can be explained by several factors. Firstly, the exposure of BEA to the air-water interface could have caused an unfolding or another structural change in the protein, leading to a loss of catalytically active protein. Likewise, a selective transfer of proteins from the Langmuir film to the solid support could have occurred, with the loss of BEA in relation to other proteins. The electrophoretic profiles (Fig. 2) showed that the protein composition of samples at the air-water interface (LF_{BEM}) differed from that of S_{BEM}, although no significant changes were observed in the region corresponding to protein bands with molecular weights like that of BEA. This would confirm the fact that BEA, because of its amphipathic nature, has a favorable tendency to remain at the air-water interface [35] and therefore to be transferred to the solid support, but in a state of lower catalytic activity.

Table 3 Kinetic parameters of acetylthiocholine hydrolysis catalyzed by BEA in BEM suspensions and in LB_{BEM} films

Enzyme source	V_{max} (nmoles P/min·µg prot)	K_M (mM)	Catalytic efficiency (V_{max}/K_M) (nmoles/(min·µg prot.mM)	*n*
S_{BEM}	3.41 ± 0.15 (4)	0.11 ± 0.02 (0.18)	0.00154	8
$LB_{MEB.10}$	0.021 ± 0.002 (9.5)	0.047 ± 0.013 (27)	0.44	5
$LB_{MEB.35}$	0.030 ± 0.003 (10)	0.026 ± 0.017 (65)	1.15	5

Numbers correspond to the mean ± s.e.m (d.f.) of *n* experiments. The incubation time was 15 min for S_{BEM} and 90 min for LB_{BEM} films. Experiments were performed at 37 ºC. The Michaelis-Menten model (Eq.2) was fitted to the experimental data. BEM, bovine erythrocyte membranes; S_{BEM}, BEM suspension; $LB_{BEM.10}$, Langmuir-Blodgett film of BEM packed at 10 mN/m; $LB_{BEM.35}$, Langmuir-Blodgett film of BEM packed at 35 mN/m.

Also, the immobilization of BEA at the solid support led to a decrease in the degrees of freedom of the enzyme movement, which may have caused a decrease in the probability of collisions with the substrate. Both the decrease in lipid diffusion coefficients, which is two times faster in a vesicle than in two-dimensional supported phospholipid bilayers [42] and the rotation of the vesicles in the incubation medium in the case of S_{BEM}, may influence the kinetics at the stage of enzyme-substrate complex (ES) formation. Diffusional restriction of the substrate cannot be responsible for the decrease in Vmax since it bears an electrostatic positive charge at physiological pH which would prevent its immobilization mediated either by hydrophobic interactions or by partitioning towards the membrane.

Another phenomenon that could affect the catalytic activity is the availability of water as a substrate for the hydrolytic reaction stage [10] if, as a hypothesis, we assume the possibility that the structure of the solvent (water) in the molecular environment of the enzyme is different in the LB_{BEM} films in comparison to S_{BEM}.

On the other hand, it should be recalled that LF_{BEM} exhibits an expanded liquid-like behavior along the entire isotherm (Figs. 4 and 5), with lateral heterogeneity, where liquid ordered (Lo) and liquid disordered (Ld) phases coexist (Fig. 6). Hence, considering that proteins with GPI anchorage in general [43, 44] and BEA in particular, tend to segregate preferentially in ordered domains [11], it is expected that BEA presents a heterogeneous distribution in the monolayer. This fact may condition the reaction kinetics if we consider the possibility that the reaction order with respect to the enzyme can be coupled to the dimensionality of the topographic distribution of the enzyme on the surface, as we demonstrated in previous works carried out with β-galactosidase in LB films [20].

Regarding the molecular packing degree in the LB_{BEM} films, it was observed that the V_{max} is higher in the $LB_{BEM,35}$ than in the $LB_{BEM,10}$. This difference could be due to the fact that a π = 35 mN/m is close to the equilibrium pressure of a bilayer [41]. Therefore, at this surface pressure, the enzyme would be in a condition that favors its native structure. It is important to bear in mind that, as stated above, it was demonstrated [11] that the membrane environment stabilized BEA from thermal denaturation.

3.4.2 K_M values in Langmuir films transferred to alkylated glasses ($LB_{BEM,10}$ and $LB_{BEM,35}$)

With respect to K_M, a conformational change could imply a more favorable exposure of the active site to the substrate, which would result in an increased apparent affinity. Moreover, a significantly lower value was obtained for K_M in $LB_{BEM,35}$ compared to $LB_{BEM,10}$. When studying the activity of immobilized enzymes, diffusional, steric and electrostatic effects must be considered. In this case, the analysis of electrostatic phenomena is of great importance because the substrate, acetylthiocholine, is positively charged at a physiological pH. In addition, the mechanism proposed for the approximation of the substrate to the active site involves interactions with negative charges present in the "deep gorge" formed in the tertiary structure of the enzyme [10]. If we assume that the increase in molecular packing induces an increase in the density of negative charges, it would be possible that in $LB_{BEM,35}$ the diffusion of the substrate towards the surface of the film is favored, which would justify a decrease in the apparent K_M of the BEA [45-47].

This hypothesis does not contradict the fact that ΔV becomes increasingly positive as the monolayer is compressed (Fig. 4) since the surface potential reflects the difference in potential between the air and the bulk solution, and is the result of a complex phenomenon of dipole reorganization that occurs at the interface during compression [46]. It is not possible to know the phenomena that occur at a molecular level in such a complex mixture as a natural membrane. However, it is possible that a positive ΔV is accompanied by an accumulation of polar groups with negative charges exposed to the interface (water side) [47], compensated by positive dipoles from other regions of the molecules. These charges could come from the sialic groups of the oligosaccharide chains of glycolipids and glycoproteins, and also due to the presence of phosphatidylserine and phosphatidylinositol [48].

3.4.3 Stability of LB films

The BEA catalytic stability of the LB_{BEM} was evaluated up to 14 days from the transference of the LF_{BEM} to the alkylated glass substrate, at 10 or 35 mN/m. The residual BEA catalytic activity was taken as a measure of stability. Results are shown in Fig. 11. The catalytic activity measured in the case of $LB_{BEM,35}$ remained constant up to day 7 and afterwards it tended to decrease. In the case of

$LB_{BEM,10}$, the activity dropped continuously from day 0, indicating that the less compact film was also the less stable.

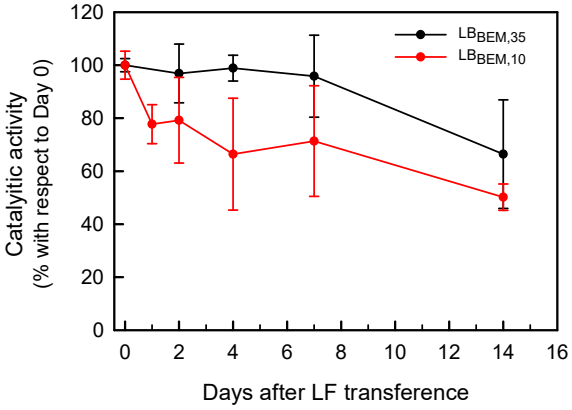

Fig.11 BEA catalytic activity vs. Days after LB_{BEM} preparation. Several $LB_{BEM,10}$ and $LB_{BEM,35}$ were transferred at day 0 and maintained under water at 4°C until the measurement of BEA catalytic activity at days 1 to 14, in the presence of 0.4 mM acetylthiocholine.

3.4.4. Effect of monoterpenes on BEA catalytic activity

Here we conducted a study about the effects of monoterpenes (MTs) on BEA activity with $LB_{BEM,35}$ as the enzyme source (Fig. 12). The results show that 1,8-cineole and eugenol produced a moderate increase in BEA activity at relatively low concentrations and a notable decrease at higher concentrations. This dual behavior, by which the effects of the compounds on AChE catalytic activity are concentration-dependent, was also described for other MTs [14].

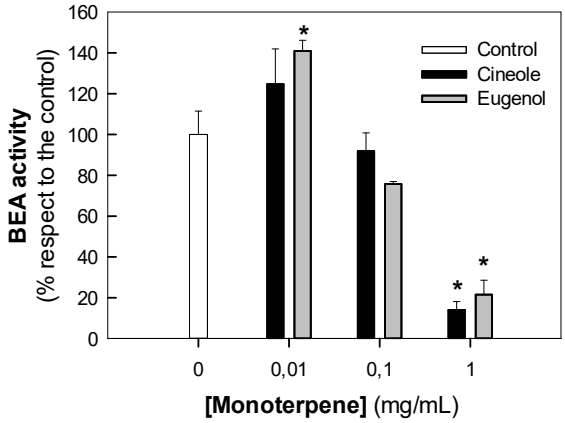

Fig. 12. Effect of monoterpenes (MTs) on the catalytic activity of BEA. Cineole and Eugenol were applied to the incubation system at the indicated concentrations. The enzyme source was $LB_{BEM,35}$. Experiments were performed at a fixed 0.4 mM substrate concentration. Control, 0 mg/mL of MT. Data correspond to the mean ± s.e.m. of triplicates. *, significantly different from the control at $p< 0.05$ (ANOVA plus Duncan post-hoc test).

In addition, the inhibitory effect of cineole and eugenol on the activity of BEA is in accordance with that described for AChEs [30, 49]. The inhibition mechanism for 1,8-Cineole is not clear and is currently under investigation in our laboratory. Miyazawa and Yamafuji [50] have proposed a competitive type inhibition mechanism on BEA while others [30] have proposed a non-competitive mechanism for human erythrocyte AChE.

However, while the previous studies on the effect of MTs on AChE were performed with a soluble enzyme purified from *Electrophorus electricus* [14] here we tested the effects of MTs on the enzyme anchored to the membrane in controlled packing conditions. It is important to highlight that MTs are hydrophobic compounds with high partition coefficients [51], capable of affecting the

membrane order and electrostatics, according to the modulus and the orientation of their dipole moment [52]. Therefore, it cannot be discarded that the partition of MTs in the membrane may affect the catalytic activity of BEA through non-specific mechanisms, considering also the ability of this enzyme to sense the dynamic state of its molecular environment.

So, LB_{BEM} represent a good experimental model that, in the future, will allow us to get deeply into the complex phenomena that modulate the catalytic activity of this membrane bound protein and the action mechanism of its inhibitors.

Several methodologies were developed in the past with the aim of sensing and quantifying the presence of organophosphate and carbamate insecticides, two classes of AChE inhibitors with high toxicity and environmentally hazardous [53]. These techniques include colorimetry, capillary electrophoresis, mass spectrometry, gas chromatography, thin layer chromatography, among others. Although these methods provided fruitful results, most of them are time-consuming and require expensive reagents and equipment [54]. On the contrary, biosensing methods provide advantages such as simplicity, sensitivity, rapidity and low cost. In particular, membrane-based AChE biosensors offer a portable, cheap and rapid method for the determination of inhibitors, enhancing the sensitivity and selectivity in comparison to other sensing methods [54]. Thus, our work constitutes a proof of concept of the feasibility of using LB_{BEM} as a prototype of biosensor for AChE inhibitors. This will be useful not only to detect the presence of contaminants, but also to perform a screening of new green pesticides like MTs, that could replace the old toxic ones.

CONCLUSIONS

Based on the results obtained in the present work we can conclude that it is possible to prepare stable Langmuir-Blodgett films from BEM preserving the catalytic activity of BEA. It is worth to note that in LB_{BEM} films, although the catalytic activity is reduced compared with S_{BEM}, we observed a significant increase in the enzyme-substrate affinity. Both parameters combined in such a manner that LB_{BEM} resulted in a higher catalytic efficiency if compared with the membrane suspension.

As expected, being BEA an anchored membrane enzyme, it was able to sense the dynamic changes that occurred in its molecular environment which were detected through the kinetics of the reaction it catalyzes. So, LB_{BEM} films constitute an appropriate model to sense the effects of the membrane molecular packing on BEA catalytic activity. Additionally, BEM is a cheap source of active enzyme.

Beyond the contribution to the understanding of BEA activity modulation, the present results show that LB_{BEM} provides a proof of concept for the development of biosensors for the screening of new green pesticides acting through acetylcholinesterase interaction. Additionally, this can be also an alternative to the electrochemical biosensors [55] for controlling the presence of forbidden pesticides such as organophosphates.

Acknowledgments

Authors acknowledge the Veterinary Dr. Jorge Carcedo, Facultad de Ciencias Agropecuarias, Universidad Nacional de Córdoba for the kindly provision of bovine blood and Dr..Benjamín Caruso who helped us with calibration of BAM images. This work was partially financed by Foncyt, Mincyt-Córdoba, SeCyT-Universidad Nacional de Córdoba and CONICET from Argentina. IF was a fellowship holder from Consejo Interuniversitario Nacional (CIN) and at present holds a fellowship from CONICET. MAP, AVT and EMC are career members of the latter institution.

Supplementary Material

Estimation of optimal incubation time and protein concentration for enzymatic assays are provided as Supplementary Material.

BIBLIOGRAPHY

[1] O. Nosjean, B. Roux, Ectoplasmic insertion of a glycosylphosphatidylinositol-anchored protein in glycosphingolipid- and cholesterol-containing phosphatidylcholine vesicles, Eur J Biochem, 263 (1999) 865-870.
[2] J. Wang, W. Gunning, K.M. Kelley, M. Ratnam, Evidence for segregation of heterologous GPI-anchored proteins into separate lipid rafts within the plasma membrane, J Membr Biol, 189 (2002) 35-43.
[3] D.B. Alberts B, L. J, R. M, K. R, W. JD, Molecular Biology of the cell, Garland Publishing, Inc., 1994.
[4] T.M. Huang, H.C. Hung, T.C. Chang, G.G. Chang, Solvent kinetic isotope effects of human placental alkaline phosphatase in reverse micelles, Biochem J, 330 (Pt 1) (1998) 267-275.
[5] R.S. Cantor, The influence of membrane lateral pressures on simple geometric models of protein conformational equilibria, Chemistry and Physics of Lipids, 101 (1999) 45-56.
[6] R.S. Cantor, Size distribution of barrel-stave aggregates of membrane peptides: influence of the bilayer lateral pressure profile, Biophysical Journal, 82 (2002) 2520-2525.
[7] E. Lauwers, R. Goodchild, P. Verstreken, Membrane Lipids in Presynaptic Function and Disease, Neuron, 90 (2016) 11-25.
[8] D.T. Auguste, J. Kirkwood, J. Kohn, F. GG., R.K. Prud'homme, Surface Rheology of Hydrophobically Modified PEG Polymers Associating with a Phospholipid Monolayer at the Air -Water Interface, Langmuir, 24 (2008) 4056-4064.
[9] I. Silman, A.H. Futerman, Modes of attachment of acetylcholinesterase to the surface membrane, Eur J Biochem, 170 (1987) 11-22.
[10] V. Nolan, P.D. Clop, M.I. Burgos, M.A. Perillo, Dual substrate/solvent- roles of water and mixed reaction-diffusion control of beta-Galactosidase catalyzed reactions in PEG-induced macromolecular crowding conditions, Biochimical and Biophysical Research Communications, (2019).
[11] D.M. Quinn, Acetylcholinesterase: enzyme structure, reaction dynamics, and virtual transition states, Chemical Reviews, 87 (1987) 955-979.
[12] J. Massoulie, S. Bon, The molecular forms of cholinesterase and acetylcholinesterase in vertebrates, Annual Review of Neuroscience, 5 (1982) 57-106.
[13] O. Jbilo, C.F. Bartels, A. Chatonnet, J.-P. Toutant, O. Lockridge, Tissue distribution of human acetylcholinesterase and butyrylcholinesterase messenger RNA, Toxicon, 32 (1994) 1445-1457.
[14] M.D. López, F.J. Campoy, M.J. Pascual-Villalobos, E. Muñoz-Delgado, C.J. Vidal, Acetylcholinesterase activity of electric eel is increased or decreased by selected monoterpenoids and phenylpropanoids in a concentrationdependent manner, Chemico-Biological Interactions, 229 (2015) 36–43.

[15] Z. Arsov, M. Schara, M. Zorko, J. Strancar, The membrane lateral domain approach in the studies of lipid-protein interaction of GPI-anchored bovine erythrocyte acetylcholinesterase, European Biophysics Journal, 33 (2004) 715-725.
[16] E.J. Frenkel, B. Roelofsen, U. Brodbeck, L.L.M. Van Deenen, P. Ott, Lipid-Protein Interactions in Human Erythrocyte-Membrane Acetylcholinesterase, European Journal of Biochemistry, 109 (1980) 377-382.
[17] A. Spinedi, P. Luly, R.N. Farias, Does the fluidity of the lipid environment modulate membrane-bound acetylcholinesterase?: Effects of temperature, membrane composition and amphiphiles, Biochemical Pharmacology, 46 (1993) 1521-1527.
[18] G.L. Gaines, Insoluble monolayers at liquid-gas interfaces, (1966).
[19] E. Clop, M.A. Perillo, Langmuir Films from Human Placental Membranes: Preparation, Rheology, Transfer to Alkylated Glasses, and Sigmoidal Kinetics of Alkaline Phosphatase in the Resultant Langmuir-Blodgett Film, Cell Biochemistry and Biophysics, 56 (2010) 91-107.
[20] E.M. Clop, P.D. Clop, J.M. Sanchez, M.a.A. Perillo, Molecular Packing Tunes the Activity of Kluyveromyces lactis β-Galactosidase Incorporated in Langmuir-Blodgett Films, Langmuir, 24 (2008) 10950-10960.
[21] J.A. Zasadzinski, R. Viswanathan, L. Madsen, J. Garnaes, D.K. Schwartz, Langmuir-Blodgett films, Science, 263 (1994) 1726-1733.
[22] C.W. Hollars, R.C. Dunn, Submicron structure in L-alpha-dipalmitoylphosphatidylcholine monolayers and bilayers probed with confocal, atomic force, and near-field microscopy, Biophys J, 75 (1998) 342-353.
[23] C.M. Rosetti, B. Maggio, R.G. Oliveira, The self-organization of lipids and proteins of myelin at the membrane interface. Molecular factors underlying the microheterogeneity of domain segregation., Biochim Biophys Acta, 1778 (2008) 1665-1675.
[24] E. Beutler, C. West, K.G. Blume, The removal of leukocytes and platelets from whole blood, J Lab Clin Med, 88 (1976) 328-333.
[25] J.T. Dodge, C. Mitchell, D.J. Hanahan, The preparation and chemical characteristics of hemoglobin-free ghosts of human erythrocytes, Archives of Biochemistry and Biophysics, 100 (1963) 119-130.
[26] O.H. Lowry, N.J. Rosebrough, A.L. Farr, R.J. Randall, Protein measurement with the Folin phenol reagent, Journal of Biological Chemistry, 193 (1951) 265-275.
[27] M.A.K. Markwell, S.M. Haas, L.L. Bieber, N.E. Tolbert, A modification of the Lowry procedure to simplify protein determination in membrane and lipoprotein samples, Analytical Biochemistry, 87 (1978) 206-210.
[28] P.S. Chen, T.Y. Toribara, H. Warner, Microdetermination of Phosphorus, Analytic Chemistry, 28 (1956) 1756-1758.
[29] V. Von Tscharner, H.M. McConnell, Physical properties of lipid monolayers on alkylated planar glass surfaces, Biophysical Journal, 36 (1981) 421-427.
[30] N.S. Perry, P.J. Houghton, A. Theobald, P. Jenner, E.K. Perry, In-vitro inhibition of human erythrocyte acetylcholinesterase by salvia lavandulaefolia essential oil and constituent terpenes, Journal of Pharmaceutics and Pharmacology, 52 (2000) 895-902.
[31] M.L. Fanani, B. Maggio, Liquid-liquid domain miscibility driven by composition and domain thickness mismatch in ternary lipid monolayers, The journal of physical chemistry. B, 115 (2011) 41-49.
[32] G.L. Ellman, K.D. Courtney, V. Andres, R.M. Featherstone, A new and rapid colorimetric determination of acetylcholinesterase activity, Biochemical Pharmacology, 7 (1961) 88-95.
[33] J.T. Davies, Interfacial phenomena 2e, Elsevier.
[34] D.C. Carrer, B. Maggio, Phase behavior and molecular interactions in mixtures of ceramide with dipalmitoylphosphatidylcholine, Journal of Lipid Research, 40 (1999) 1978-1989.
[35] L. Dziri, S. Boussaad, S. Wang, R.M. Leblanc, Surface topography of acetylcholinesterase in Langmuir and Langmuir-Blodgett films, The Journal of Physical Chemistry B, 101 (1997) 6741-6748.
[36] R.G. Oliveira, R.O. Calderon, B. Maggio, Surface behavior of myelin monolayers, Biochimica et Biophysica Acta, 1370 (1998) 127-137.

[37] A.V. Turina, P.D. Clop, M.A. Perillo, Synaptosomal membrane-based Langmuir-Blodgett films: a platform for studies on gamma-aminobutyric acid type A receptor binding properties, Langmuir, 31 (2015) 1792-1801.
[38] E.M. Clop, N.A. Corvalán, M.A. Perillo, Langmuir films of dipalmitoyl phosphatidylethanolamine grafted poly(ethylene glycol). In-situ evidence of surface aggregation at the air-water interface, Colloids and Surfaces B: Biointerfaces, 148 (2016) 640-649.
[39] T. Baumgart, G. Hunt, E.R. Farkas, W.W. Webb, G.W. Feigenson, Fluorescence probe partitioning between L o/L d phases in lipid membranes, Biochimica et Biophysica Acta (BBA)-Biomembranes, 1768 (2007) 2182-2194.
[40] E. D'Imprima, D. Floris, M. Joppe, R. Sánchez, M. Grininger, W. Kühlbrandt, Protein denaturation at the air-water interface and how to prevent it, Elife, pii: e42747 (2019).
[41] C.M. Rosetti, B. Maggio, R.G. Oliveira, The self-organization of lipids and proteins of myelin at the membrane interface. Molecular factors underlying the microheterogeneity of domain segregation, Biochimica et Biophysica Acta (BBA)-Biomembranes, 1778 (2008) 1665-1675.
[42] M. Przybylo, J. SÃ½kora, J. HumpolÃ-cÌŒkovÃ¡, A. Benda, A. Zan, M. Hof, Lipid diffusion in giant unilamellar vesicles is more than 2 times faster than in supported phospholipid bilayers under identical conditions, Langmuir, 22 (2006) 9096-9099.
[43] O. Nosjean, B. Roux, Ectoplasmic insertion of a glycosylphosphatidylinositol-anchored protein in glycosphingolipid- and cholesterol-containing phosphatidylcholine vesicles, European Journal of Biochemistry, 263 (1999) 865-870.
[44] J. Wang, W. Gunning, K.M. Kelley, M. Ratnam, Evidence for segregation of heterologous GPI-anchored proteins into separate lipid rafts within the plasma membrane, Journal of Membrane Biology, 189 (2002) 35-43.
[45] P. Ott, Membrane acetylcholinesterases: purification, molecular properties and interactions with amphiphilic environments, Biochimica et Biophysica Acta (BBA)-Reviews on Biomembranes, 822 (1985) 375-392.
[46] V. Vogel, D. Moebius, Local surface potentials and electric dipole moments of lipid monolayers: contributions of the water/lipid and the lipid/air interfaces, Journal of Colloid and Interface Science, 126 (1988) 408-420.
[47] H. Brockman, Dipole potential of lipid membranes, Chemistry and Physics of Lipids, 73 (1994) 57-79.
[48] D.J. Hanahan, R.M. Watts, D. Pappajohn, Some chemical characteristics of the lipids of human and bovine erythrocytes and plasma, Journal of lipid research, 1 (1960) 421-432.
[49] S. Dohi, M. Terasaki, M. Makino, Acetylcholinesterase inhibitory activity and chemical composition of commercial essential oils, Journal of agricultural and food chemistry, 57 (2009) 4313-4318.
[50] M. Miyazawa, C. Yamafuji, Inhibition of acetylcholinesterase activity by tea tree oil and constituent terpenoids. , Flavour and Fragrance Journal, 21 (2006) 198-201.
[51] A.V. Turina, M.V. Nolan, J.A. Zygadlo, M.A. Perillo, Natural terpenes: self-assembly and membrane partitioning, Biophysical Chemistry, 122 (2006) 101-113.
[52] M.P. Zunino, A.V. Turina, J.A. Zygadlo, M.A. Perillo, Stereoselective effects of monoterpenes on the microviscosity and curvature of model membranes assessed by DPH steady-state fluorescence anisotropy and light scattering analysis, Chirality, 23 (2011) 867-877.
[53] S. Chapalamadugu, G.R. Chaudhry, Microbiological and biotechnologicalaspects of metabolism of carbamates and organophosphates, Critical Reviews in Biotechnology, 12 (1992) 357–389.
[54] C.S. Pundir, N. Chauhan, Acetylcholinesterase inhibition-based biosensors for pesticide determination: A review, Analytical Biochemistry, 429 (2012) 19-31.
[55] V. Dhull, A. Gahlaut, N. Dilbaghi, V. Hooda, Acetylcholinesterase Biosensors for Electrochemical Detection of Organophosphorus Compounds: A Review, Biochemistry Research International, 731501 (2013).

Biochimica et Biophysica Acta (BBA) - Biomembranes.
Volume 1862, Issue 5, 1 May 2020, 183188
https://doi.org/10.1016/j.bbamem.2020.183188

SUPPORTING INFORMATION

Sensing molecular organizational changes through the catalytic activity of acetylcholinesterase from erythrocyte membranes in Langmuir-Blodgett films.

Iván Felsztyna[1,2], María A. Perillo[1,2,*], and Eduardo M. Clop[1,2,*]

[1] Universidad Nacional de Córdoba, Facultad de Ciencias Exactas, Físicas y Naturales. Departamento de Química, Cátedra de Química Biológica. Córdoba, Argentina.

[2] CONICET, Instituto de Investigaciones Biológicas y Tecnológicas (IIByT). Córdoba, Argentina

*Co-Corresponding authors e-mail: eduardo.clop@unc.edu.ar; mperillo@unc.edu.ar

CONTENTS (S1 to S3 refer to page numbers)

Biochimica et Biophysica Acta (BBA) - Biomembranes.
Volume 1862, Issue 5, 1 May 2020, 183188
https://doi.org/10.1016/j.bbamem.2020.183188

Determination of the optimal incubation time for BEA activity assays in membranes suspensions and in Langmuir-Blodgett films

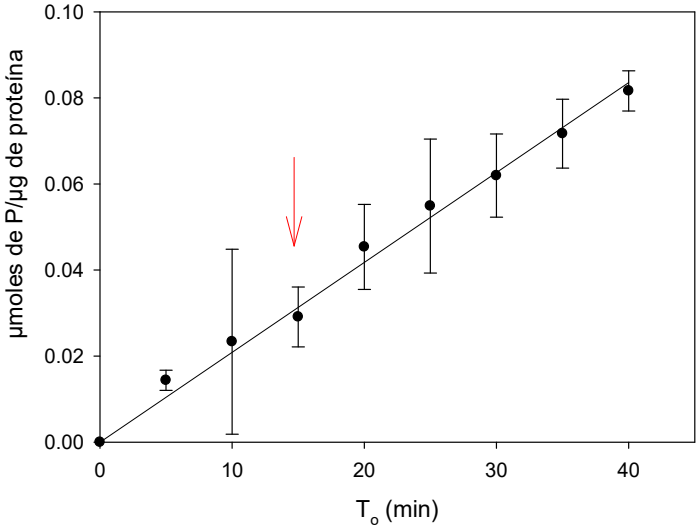

Fig. S1: BEA catalytic activity as a function of incubation time using S_{BEM} as the enzyme source. The red arrow indicates the incubation time that was selected for substrate concentration assays (15 min).

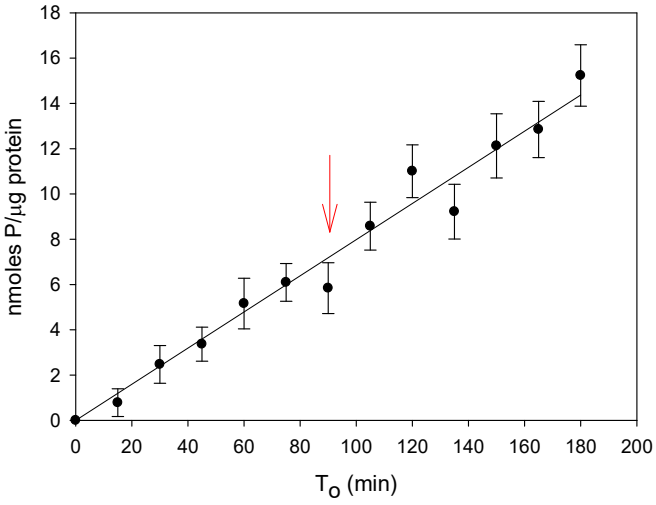

Fig. S2: BEA catalytic activity as a function of incubation time using LB_{BEM35} as the enzyme source. The red arrow indicates the incubation time that was selected for substrate concentration assays (90 min).

Biochimica et Biophysica Acta (BBA) - Biomembranes.
Volume 1862, Issue 5, 1 May 2020, 183188
https://doi.org/10.1016/j.bbamem.2020.183188

Determination of the optimal protein cocentration for BEA activity assays

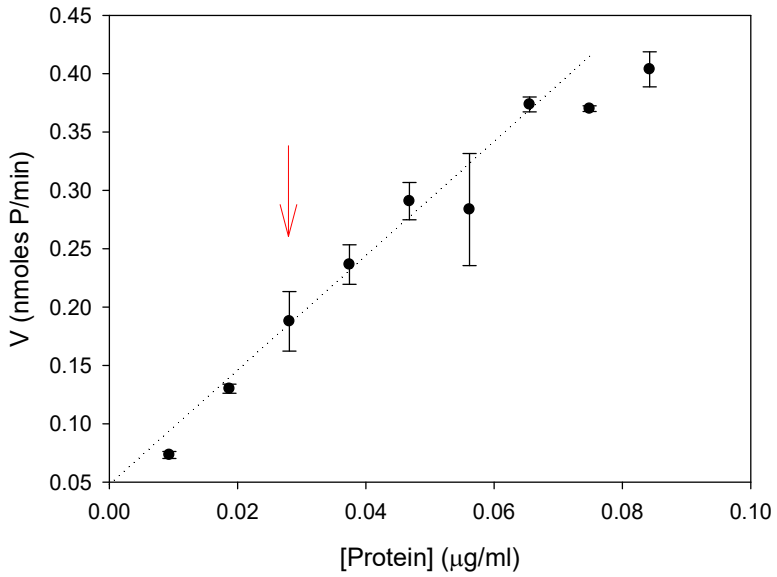

Fig. S3: BEA catalytic activity as a function of protein concentration using S_{BEM} as the enzyme source. The red arrow indicates the concentration that was selected for substrate concentration assays.